Fabrication of $LiCoO_2$/Helical Nanocarbon Composites and Their Effect on Lithium Cell Performance

Toshiro Hirai[a, c, *], Toshihiro Yoshida[a], Yusuke Uno[a,d], and Tomonobu Tsujikawa[b]

[a] Department of Mechanical Systems Engineering, Toyama Prefectural University, Imizu-shi, Toyama-ken 939-0398, Japan

[b] NTT Facilities, Inc., Toshima-ku, Tokyo 170-0004, Japan

[c] Present address; SACI, Kyoto University, Nishikyo-ku, Kyoto 615-8520, Japan

[d] Present address; Chuo Branch, NTT Facilities, Inc., Minato-ku, Tokyo 108-0023, Japan

* Corresponding author

E-mail address: t-hirai@saci.kyoto-u.ac.jp

Fax: +81-75-383-3048

Phone: +81-75-383-3052

Abstract

We fabricate $LiCoO_2$/helical nanocarbon (HCN) composites by forming HCNs on $LiCoO_2$ on which iron oxides (Fe_2O_3 or Fe_3O_4) are dispersed ($LiCoO_2(Fe_2O_3)$ or $LiCoO_2(Fe_3O_4)$) as catalysts for HCN formation, and estimate their electrochemical properties. Granular nanocarbons form on $LiCoO_2(Fe_2O_3)$ and $LiCoO_2(Fe_3O_4)$ at 350^{o}C although HCNs of about 100 nm in diameter form on $LiCoO_2(Fe_2O_3)$ at 450^{o}C. Transmission electron microscopy and energy dispersive x-ray spectroscopy measurements show that HCNs consist of stacked graphene layers for $LiCoO_2(Fe_2O_3)$/HCN composites fabricated at 450^{o}C. On the other hand, several-nm-thick tetragonal layer exists on the $LiCoO_2$ substrate and amorphous nanocarbons form on the tetragonal layer for $LiCoO_2(Fe_2O_3)$/HCN and $LiCoO_2(Fe_3O_4)$/HCN composites fabricated at 350^{o}C. X-ray diffraction measurements suggest that Fe_2O_3 and Fe_3O_4 do not completely inhibit $LiCoO_2$ decomposition. Cathodes containing $LiCoO_2(Fe_2O_3)$/HCN or $LiCoO_2(Fe_3O_4)$/HCN fabricated at 350^{o}C improve rate capability of lithium cells. However, this rate capability is not better than that of cathodes containing a mixture of $LiCoO_2$ and acetylene black.

Introduction

High-rate and long-life lithium-ion batteries have long been expected as automotive and next-generation industrial batteries. Cathode active material/carbon composites have been studied as means of prolonging cycle life of such batteries (1, 2) as well as cathode active materials have been studied to improve lithium-ion cell capacity and rate capability (3-7).

On the other hand, some researchers have fabricate nanocarbons using chemical vapor deposition (CVD) (8-11). Nanocarbons produced using CVD has a helical shape and are reported to be semimetals with the potential to be superconductive materials (12). This suggests that they have high potential for use as conductive materials for the cathodes of lithium-ion cells. We have fabricated $LiCoO_2$/helical nanocarbon (HCN) composites and evaluated their electrochemical properties (13). We successfully obtained composites from HCNs formed on a $LiCoO_2$ substrate. However, $LiCoO_2$ severely decomposed and a cell containing $LiCoO_2$/HCN composite exhibited a low specific capacity.

We used Fe_2O_3 and Fe_3O_4 as catalysts to fabricate $LiCoO_2$/HCNs effectively without $LiCoO_2$ decomposition at lower temperature to show better performance as cathode active material. We prepared a $LiCoO_2$ substrate on which iron oxides (Fe_2O_3 or Fe_3O_4) were dispersed ($LiCoO_2(Fe_2O_3)$ or $LiCoO_2(Fe_3O_4)$) as catalysts for HCN formation. We then formed HCNs on $LiCoO_2(Fe_2O_3)$ or $LiCoO_2(Fe_3O_4)$ at 450^oC or lower and estimated effect of the composites on lithium cell performance.

Experimental

We used $LiCoO_2$ (Nippon Chemical Industrial Co., Diameter: 10μm) as a substrate and Fe_2O_3 and Fe_3O_4 (Wako Pure Chemical Industries, Ltd.) as catalysts for helical nanocarbon (HCN) formation using chemical vapor deposition (CVD).

We prepared slurries by dispersing 10 g of $LiCoO_2$ and 0.5 g of Fe_2O_3 or Fe_3O_4 into 50 ml of distilled water to uniformly and effectively disperse Fe_2O_3 or Fe_3O_4 on the surface of $LiCoO_2$ particles and stirred a solution containing the mixture in a beaker overnight on a hot plate at about 80^{o}C to evaporate water. The mixture was then dried overnight in a vacuum at 80^{o}C.

We fabricated the composites by forming HCNs on the surface of $LiCoO_2/Fe_2O_3$ or $LiCoO_2/Fe_3O_4$ powder mounted on a ceramic boat using CVD in a quartz tube and supplied 60 ml min^{-1} of C_2H_2 gas as a carbon source and 50 ml min^{-1} of Ar as a carrier at 450ºC or 350^{o}C for 10 min.

We estimated the electrochemical properties of the composites using a lithium cell. We fabricated cathode disks (area, 1.33 cm^2) by mixing the obtained composites, acetylene black (AB, Denki Kagaku Kogyo Co.) and PTFE powder with a ratio of 70 wt% of $LiCoO_2$, 25 wt% of AB and HCNs formed using CVD, and 5 wt% of PTFE, and rolling the mixture into a flat sheet. We fabricated CR2032 coin-type cells for evaluating electrochemical properties. Each coin-type cell consisted of a cathode, a lithium anode (Honjo Chemical Co.: area, 1.13 cm^2) and a 1 M $LiPF_6$-ethylene carbonate/dimethyl carbonate (volume ratio: 1/1) electrolyte (Tomiyama Pure

Chemicals Co.). Test cells were charged at 0.75 mA cm^{-2} to 4.3 V and then discharged at constant current to 3.0 V at 21^{o}C after a 10-min rest.

Results and Discussion

Figure 1 shows a scanning electron microscope (SEM) image of the $LiCoO_2$/HCN composite. HCNs are formed on the $LiCoO_2$ surface. However, the HCNs are not distributed uniformly and the bare $LiCoO_2$ surface can be seen. HCNs have a helical shape with a diameter of 200 nm or smaller. We generally observed HCNs with an irregular helical shape. We have not found an optimum fabrication condition of HCNs with a regular helical shape.

Figure 2 shows transmission electron microscope (TEM) photos of the composites fabricated from HCNs formed on $LiCoO_2$ substrate without iron oxides at 450^{o}C. HCNs contain many crystalline boundaries of graphene layers and serious turbulence was also observed, indicated with the circle in Fig. 2, which may result in an irregular helical shape of HCNs. We measured contents of the composites by energy dispersive x-ray spectroscopy (EDS). Figure 3 shows areas for EDS measurements as squares. The results are listed in Table 1. Carbon mainly existed in dark areas 1, 2, 3, and 4 around the white area. On the other hand, white area 5 contained more than 60% Co, which is larger than the Co percentage of $LiCoO_2$. This suggests that area 5 contained Co and CoO formed from decomposed $LiCoO_2$.

Furthermore, we used X-ray diffraction (XRD) to estimate the stability of $LiCoO_2$ under our experimental conditions. Figure 4 shows XRD patterns of $LiCoO_2$/HCN composites fabricated at

450°C. The XRD contains peaks of Li_2CO_3, Co, and CoO and no peaks of $LiCoO_2$, which shows that $LiCoO_2$ decomposed without iron oxides. The results coincide with those of EDS measurements.

We then fabricated a composite from HCNs formed on $LiCoO_2$ substrate with Fe_2O_3 or Fe_3O_4 and estimate its effect on inhibition of $LiCoO_2$ decomposition. Figure 5 shows SEM photo of the composite fabricated with Fe_2O_3 at 450°C. HCNs were successfully formed on $LiCoO_2$ particles and there was no significant difference in the HCN formation from the composites fabricated without iron oxides. We obtained the same results for the composite fabricated with Fe_3O_4. On the other hand, we observed nanocarbons were not helical shaped for the composites fabricated at 350°C (Fig. 6). “Immature” and particulate HCNs formed on the substrate at 350°C.

Figure 7 shows TEM photos of the composite fabricated with Fe_2O_3 at 350°C. Figure 7(a) shows TEM image of the area where there was Fe_2O_3, and Fig. 7(b) shows TEM image of the area where there was no Fe_2O_3.

By fabricating at 350°C, amorphous nanocarbons (C in Fig. 7), formed on the $LiCoO_2$ substrate (A in Fig. 7), and there was no significant difference in shape due to the existence of Fe_2O_3. We also observed a tetragonal thin layer (B in Fig. 7) on the substrate A. Figure 8 shows TEM photos of the composite fabricated with Fe_3O_4 at 350°C. We observed the same condition for the composite fabricated with Fe_3O_4 at 350°C shown in both of Fig. 8 (a) and (b) as that for the composite fabricated with Fe_2O_3 at 350°C.

We observed a tetragonal layer on as-received $LiCoO_2$ particles. We therefore do not conclude that this layer formed using CVD. Kobayashi et al. reported a layer on $Li(NiCo)O_2$ (14), which corresponds to what we observed.

Figure 9 shows XRD patterns of $LiCoO_2$/nanocarbon composites prepared with and without Fe_2O_3; $LiCoO_2(Fe_2O_3)$/HCN (350^oC), $LiCoO_2(Fe_2O_3)$/HCN (450^oC), and $LiCoO_2$/HCN (450^oC). The XRD patterns indicate that $LiCoO_2$ retained its original structure in part but it also suggests that addition of Fe_2O_3 did not prevent $LiCoO_2$ from decomposing.

We also measured XRD for $LiCoO_2(Fe_3O_4)$/HCN composite fabricated at 350^oC and confirmed addition of Fe_3O_4 inhibited $LiCoO_2$ decomposition through HCN fabrication.

We evaluated $LiCoO_2$ decomposition in relation to the addition of Fe_2O_3 and HCN fabrication temperature. Table 2 shows intensity ratios of main peaks of Li_2CO_3 (peak B in Fig. 9), CoO (peak C in Fig. 9), and Co (peak D in Fig. 9) based on $LiCoO_2$ peak (peak A in Fig. 9). XRD peak intensity ratios indicate that $LiCoO_2$ decomposition was significantly inhibited by coating with Fe_2O_3 and that HCN fabrication temperature decreased.

We estimated the electrochemical properties of $LiCoO_2$/nanocarbon composites using a lithium cell. Figure 10 shows rate capability of lithium cells containing $LiCoO_2(Fe_2O_3)$/HCN composites, $LiCoO_2(Fe_2O_3)$/HCN (350^oC) and $LiCoO_2(Fe_2O_3)$/HCN (450^oC), compared with that of a lithium cell containing as-received $LiCoO_2$. The cell containing $LiCoO_2(Fe_2O_3)$/HCN (350^oC) showed better rate capability than cell containing $LiCoO_2(Fe_2O_3)$/HCN (450^oC). However, the rate

capability of our composites is currently inferior to that of as-received $LiCoO_2$. We also estimated the rate capability of a lithium cell containing $LiCoO_2(Fe_3O_4)$/HCN composite (350^oC). The results are shown in Fig. 11. The $LiCoO_2(Fe_3O_4)$/HCN (350^oC) cell showed the same rate capability as the $LiCoO_2(Fe_2O_3)$/HCN (350^oC) cell. By using iron oxide catalysts and fabricating the composites at lower temperature, $LiCoO_2$ decomposed less and the composites showed better cell performance than that of composites fabricated without the catalysts at higher temperature. The challenge is to fabricate composites with more crystallized HCN for better rate capability of lithium cells than that of the cathode mixed with $LiCoO_2$ and AB.

Conclusion

We fabricated $LiCoO_2$/helical nanocarbon (HCN) composites by forming HCNs on $LiCoO_2$ on which iron oxides (Fe_2O_3 or Fe_3O_4) were dispersed ($LiCoO_2(Fe_2O_3)$ or $LiCoO_2(Fe_3O_4)$) as catalysts for HCN formation, and estimated their electrochemical properties.

Cathode active material/nanocarbon composites were fabricated by forming HCNs on $LiCoO_2$ coated with iron oxides (Fe_2O_3 or Fe_3O_4) to inhibit $LiCoO_2$ degradation. The following results were obtained:

(1) Granular nanocarbons were generated on $LiCoO_2$ with Fe_2O_3 and $LiCoO_2$ with Fe_3O_4 at 350^{o}C although HCNs with about 100 nm diameter were generated on $LiCoO_2$ with Fe_2O_3 at 450^{o}C.

(2) TEM measurements showed that HCNs consisted of stacked graphene layers for $LiCoO_2$/HCN fabricated at 450^{o}C. On the other hand, several-nm-thick tetragonal layer existed on the $LiCoO_2$ and amorphous nanocarbons formed on the tetragonal layer for $LiCoO_2(Fe_2O_3)$/HCN and $LiCoO_2(Fe_3O_4)$/HCN composites fabricated at 350^{o}C.

(3) XRD measurements suggested that Fe_2O_3 and Fe_3O_4 did not completely inhibit $LiCoO_2$ decomposition.

(4) Cathodes containing $LiCoO_2(Fe_2O_3)$/HCN or $LiCoO_2(Fe_3O_4)$/HCN composites fabricated at 350^{o}C improved rate capability, but this capability is not as good as that of cathodes containing a mixture of $LiCoO_2$ and AB.

Acknowledgments

The authors thank Nippon Chemical Industrial, Co. Ltd. for providing cathode active materials.

References

1. H. Huang, S-C. Yin, and L. F. Nazar, Electrochem. Solid-State Lett., 4 (2001) A170.
2. M. Tabuchi, Y. Nabeshima, K. Ado, T. Takeuchi, M. Shikano, H. Kageyama, and K. Tatsumi, Extended Abstract for the 47th Battery Symposium in Japan, Tokyo, 2D19, 2006, pp. 362–363 (in Japanese).
3. T. Ohzuku and Y. Makimura, Chem. Lett., 30 (2001) 642.
4. A. K. Padhi, K. S. Nanjundaswamy, and J. B. Goodenough, J. Electrochem. Soc., 144 (1997) 1188.
5. K. Amine, H. Yasuda, and M. Yamachi, Electrochem. Solid State Lett., 3 (2000) 178.
6. A. Yamada, S. C. Chung, and K. Hinokuma, J. Electrochem. Soc., 148 (2001) A224.
7. A. S. Andersson, J. O. Thomas, B. Kalsa, and L. Haggstroem, Electrochem. Solid-State Lett., 3 (2000) 66.
8. R. T. K. Baker and J. J. Chludzinski, Jr., J. Catal., 64 (1980) 464.
9. S. Amelinckx, X. B. Zhang, D. Bernaerts, X. F. Zhang, V. Ivanov, and J. B. Nagy, Science, 265 (1994) 635.
10. M. Zhang, Y. Nakayama, and L. Pan, Jpn. J. Appl. Phys., 39 (2000) L1242.
11. L. Pan, M. Zhang, and Y. Nakayama, Jpn. J. Appl. Phys., 91 (2002) 10058.
12. K. Akagi, R. Tamura, and M. Tsukada, Phys. Rev. Lett., 74 (1995) 2307.
13. Y. Uno, T. Tsujikawa, and T. Hirai, J. Power Sources, 195 (2010) 354.

14. H. Kobayashi, M. Shikano, S. Koike, H. Sakaebe, and K. Tatsumi, J. Power Sources, 174 (2007) 380.

Table 1 Results of EDS measurements

Area	Amount of atoms (%)			
	C	O	Co	Total
1	99.52	0.41	0.06	100.00
2	99.04	0.74	0.22	100.00
3	89.96	5.94	4.10	100.00
4	99.64	0.28	0.09	100.00
5	25.92	11.27	62.80	100.00

Table 2 XRD peak intensity ratio for $LiCoO_2$/nanocarbon composites

Composite	A/B	A/C	A/D
$LiCoO_2(Fe_2O_3)$/HCN (350^oC)	10.37	335.8	386.7
$LiCoO_2(Fe_2O_3)$/HCN (450^oC)	11.86	4.123	17.34
$LiCoO_2$/HCN (450^oC)	1.984	1.051	0.0313

Figure Captions

Fig. 1 SEM image of $LiCoO_2$/HCN composites fabricated at 450^oC for 10 min

Fig. 2 TEM image of $LiCoO_2$/HCN composite fabricated at 450^oC for 10 min

Fig. 3 TEM image of $LiCoO_2$/HCN composite fabricated at 450^oC for 10 min, and areas for EDS measurements

Fig. 4 XRD patterns of $LiCoO_2$/HCN (450^oC)

Fig. 5 SEM photo of $LiCoO_2(Fe_2O_3)$/HCN fabricated at 450^oC

Fig. 6 SEM photo of $LiCoO_2(Fe_2O_3)$/nanocarbon fabricated at 350^oC

Fig. 7 TEM images of $LiCoO_2(Fe_2O_3)$/nanocarbon composites fabricated at 350^oC for 10 min.

A: $LiCoO_2$ substrate, B: tetragonal layer, C: nanocarbon fabricated using CVD, and D: deposited Ti layer for TEM measurements

Fig. 8 TEM images of $LiCoO_2(Fe_3O_4)$/nanocarbon composites fabricated at 350^oC for 10 min.

A: $LiCoO_2$ substrate, B: tetragonal layer, C: nanocarbon fabricated by CVD, and D: deposited Ti layer for TEM measurements

Fig. 9 XRD patterns of $LiCoO_2$/nanocarbon composites fabricated with and without Fe_2O_3

Fig. 10 Rate capability of lithium cells containing $LiCoO_2(Fe_2O_3)$/HCN composite and cell containing as-received $LiCoO_2$

Fig. 11 Rate capability of lithium cells containing $LiCoO_2(Fe_2O_3)$/HCN and $LiCoO_2(Fe_3O_4)$/HCN composites fabricated at 350^oC

Fig. 1

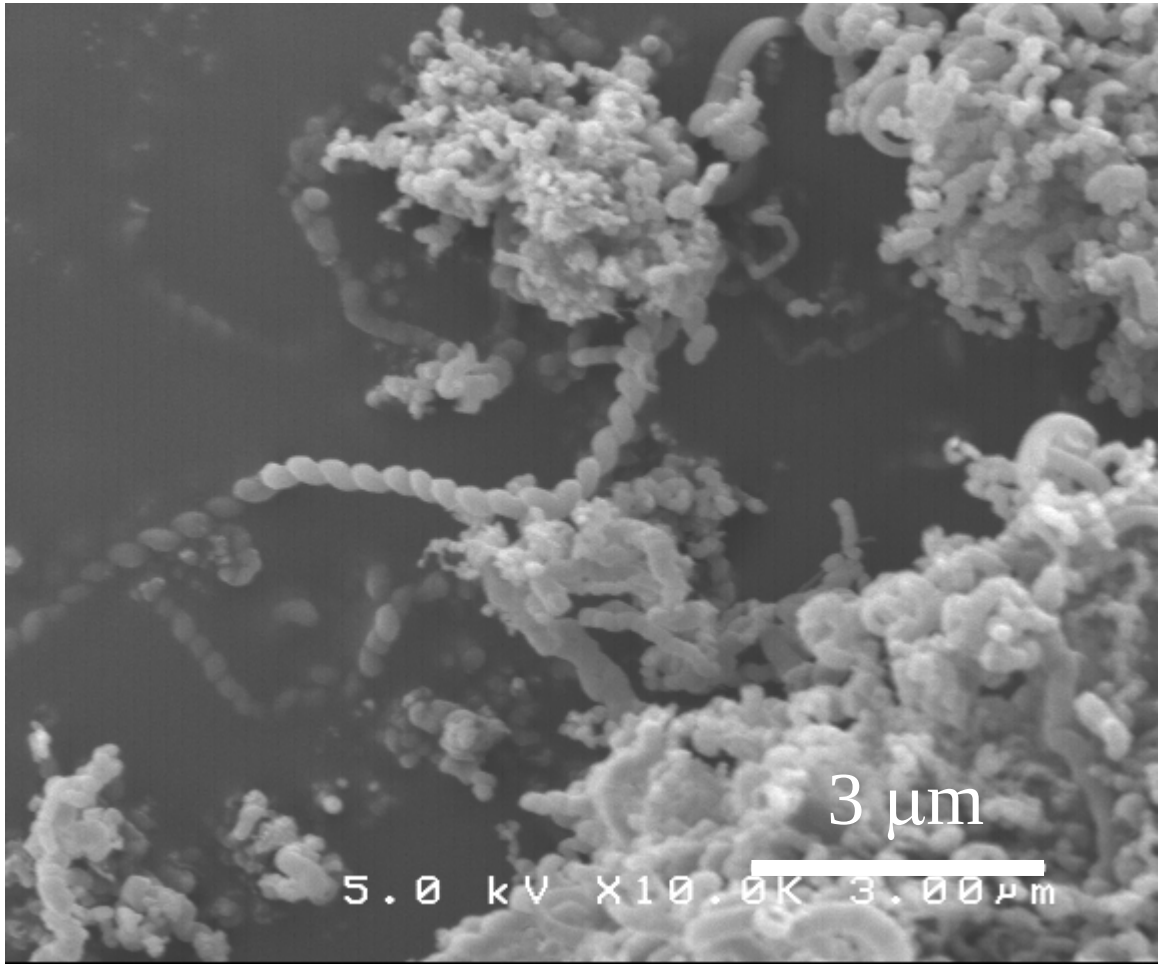

Fig. 2

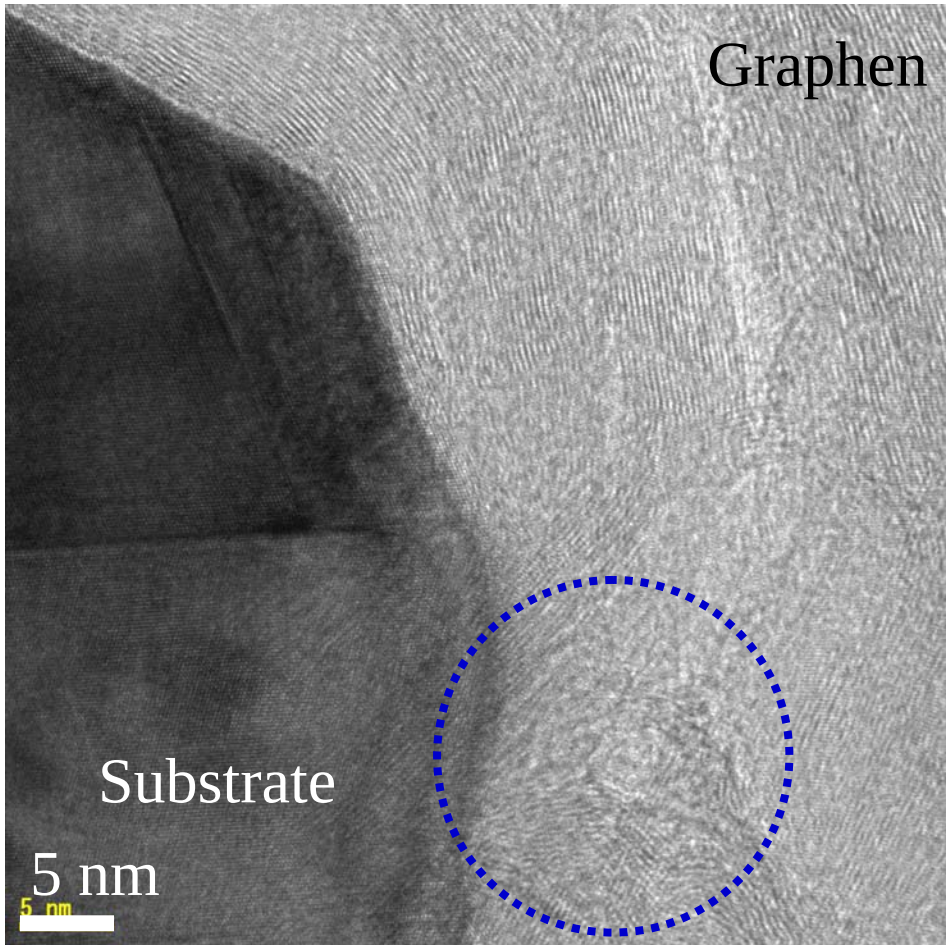

Fig. 3

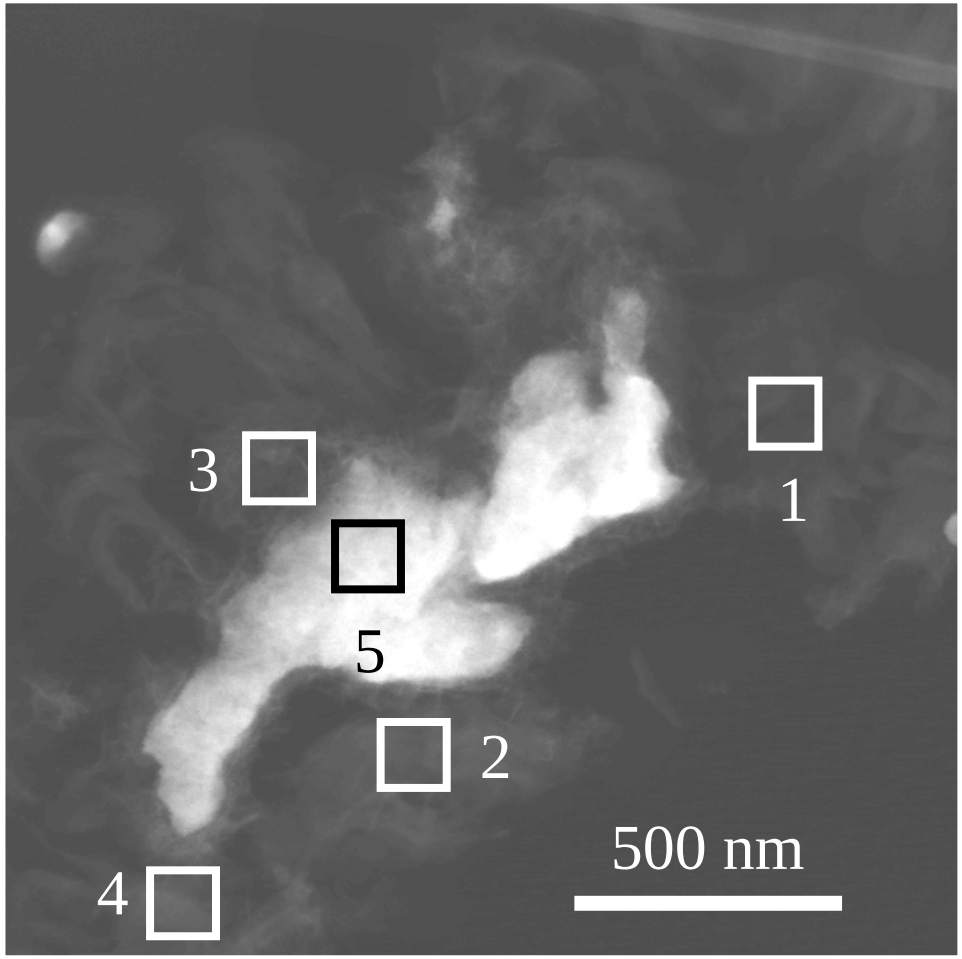

Fig. 4

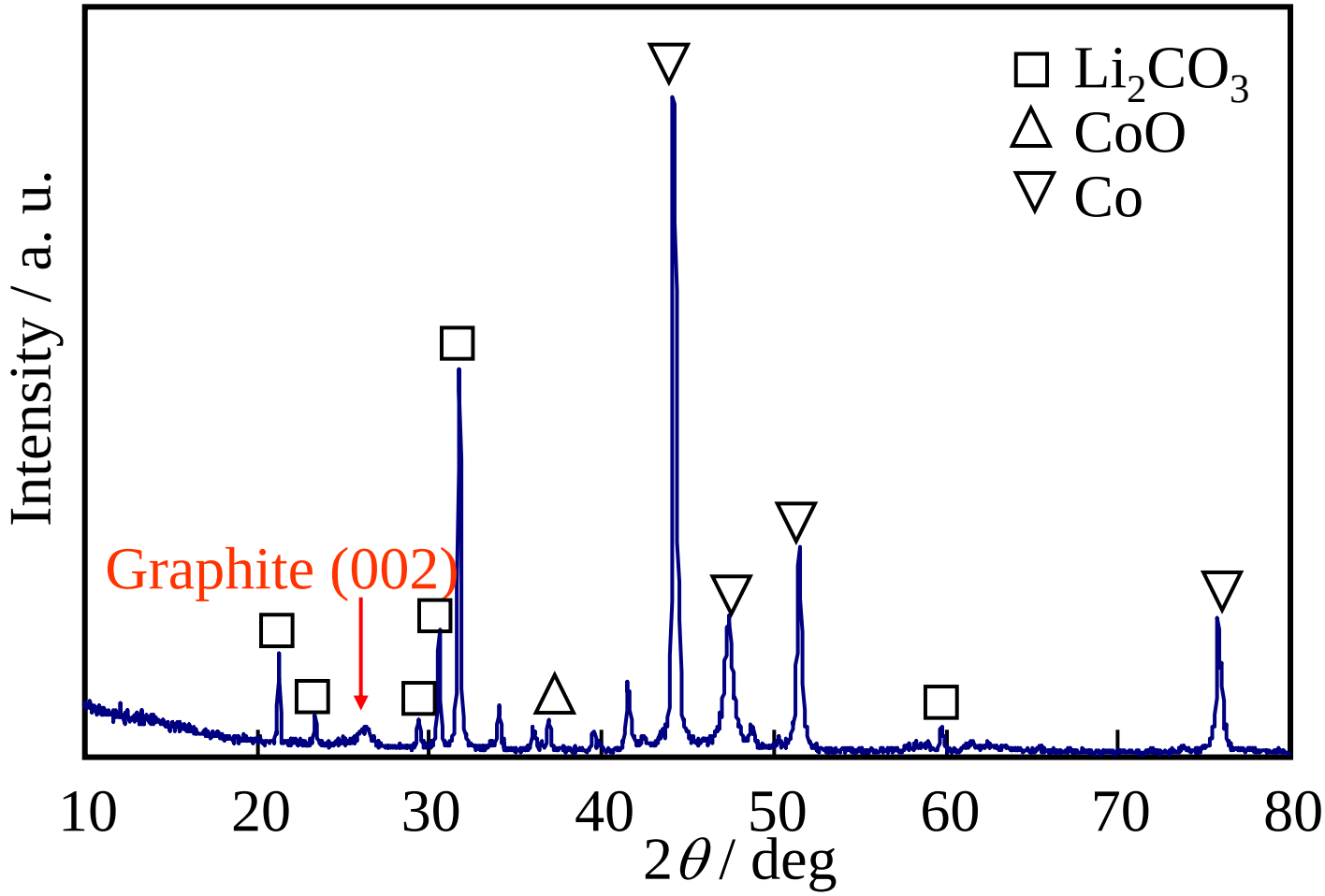
Intensity / a. u.
□ Li2CO3
△ CoO
▽ Co
Graphite (002)
10
20
30
40
50
60
70
80
2θ / deg

Fig. 5

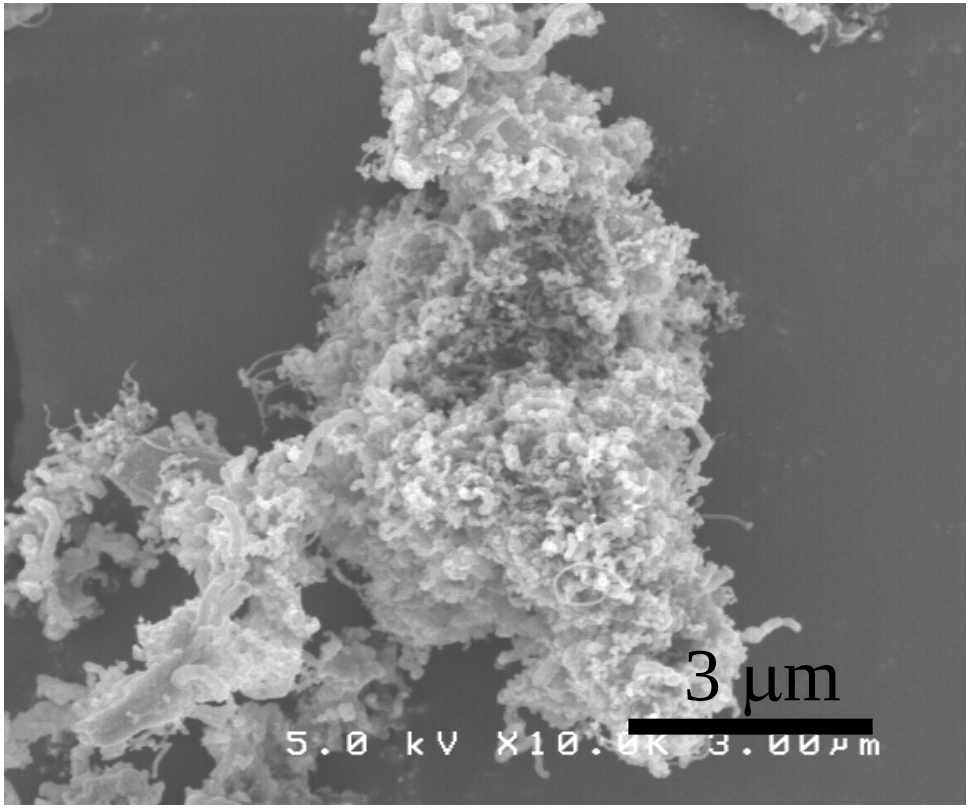

Fig. 6

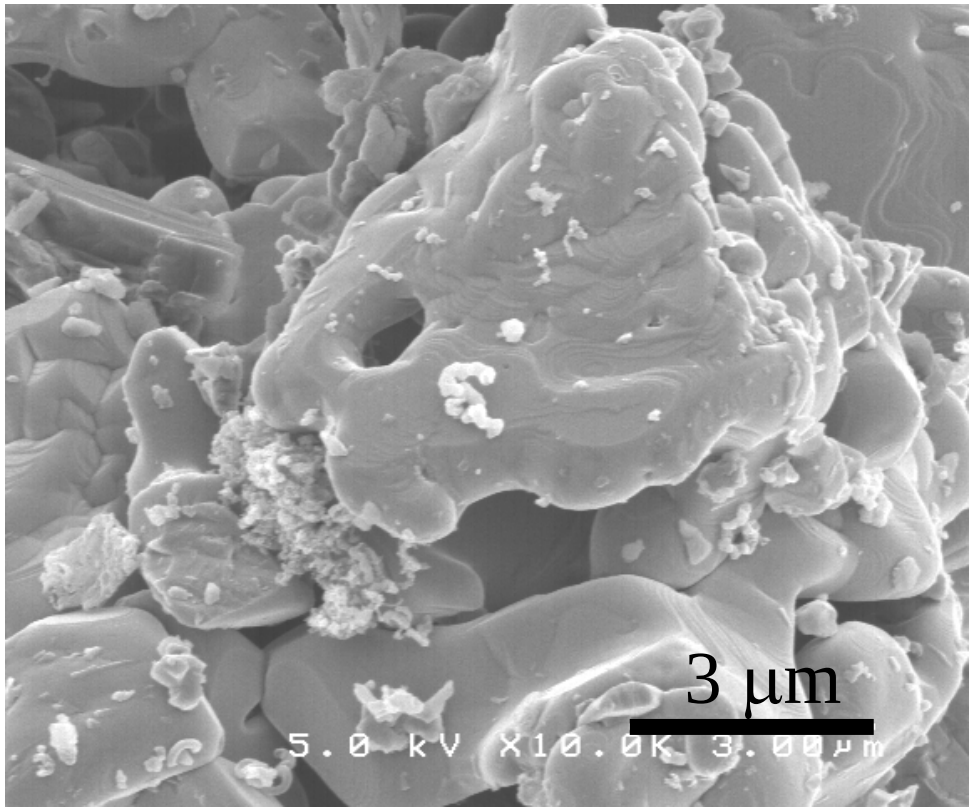

Fig. 7

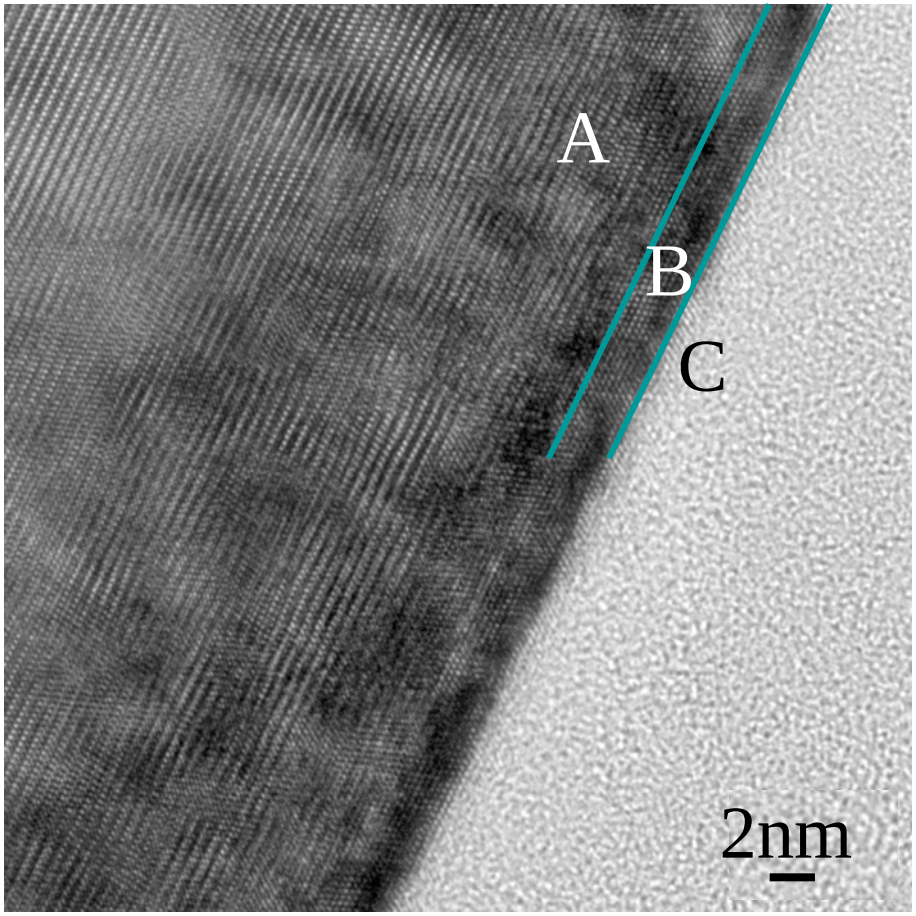

(a)

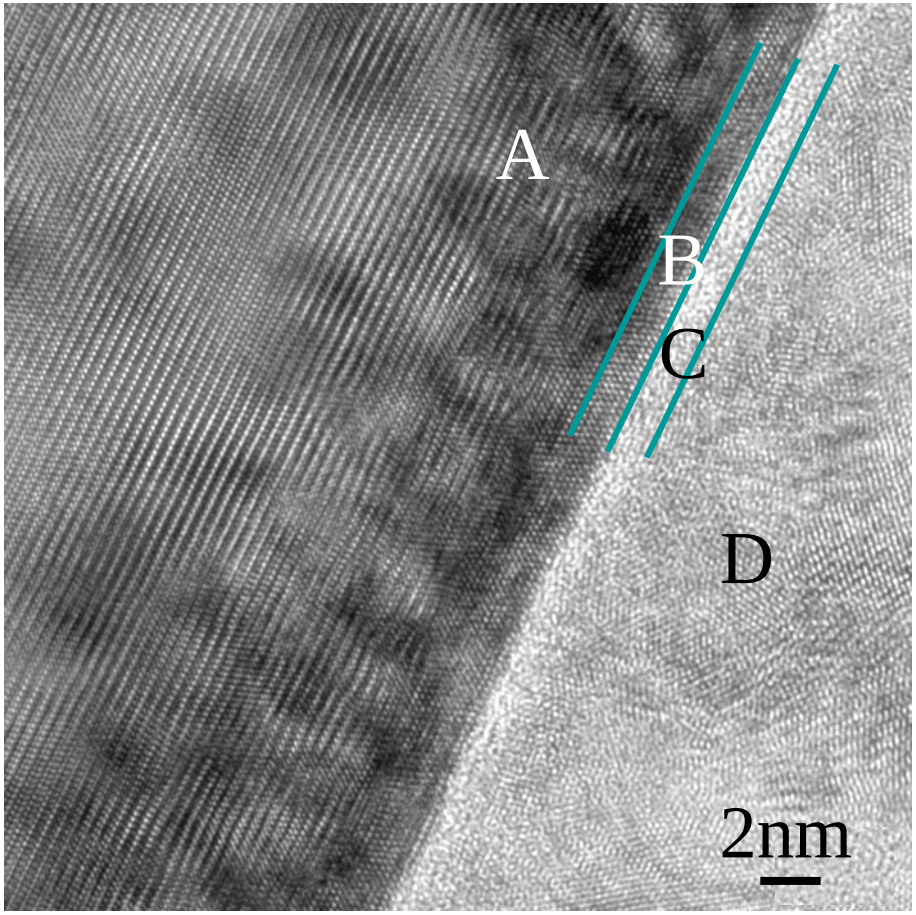

(b)

Fig. 8

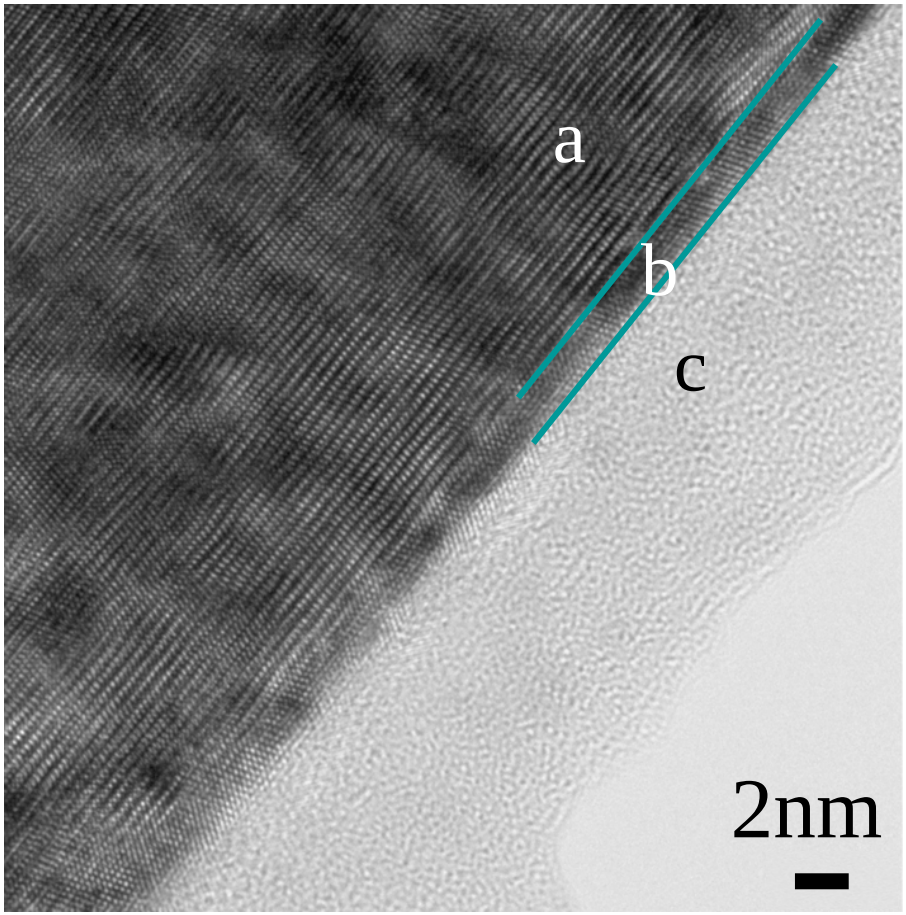

(a)

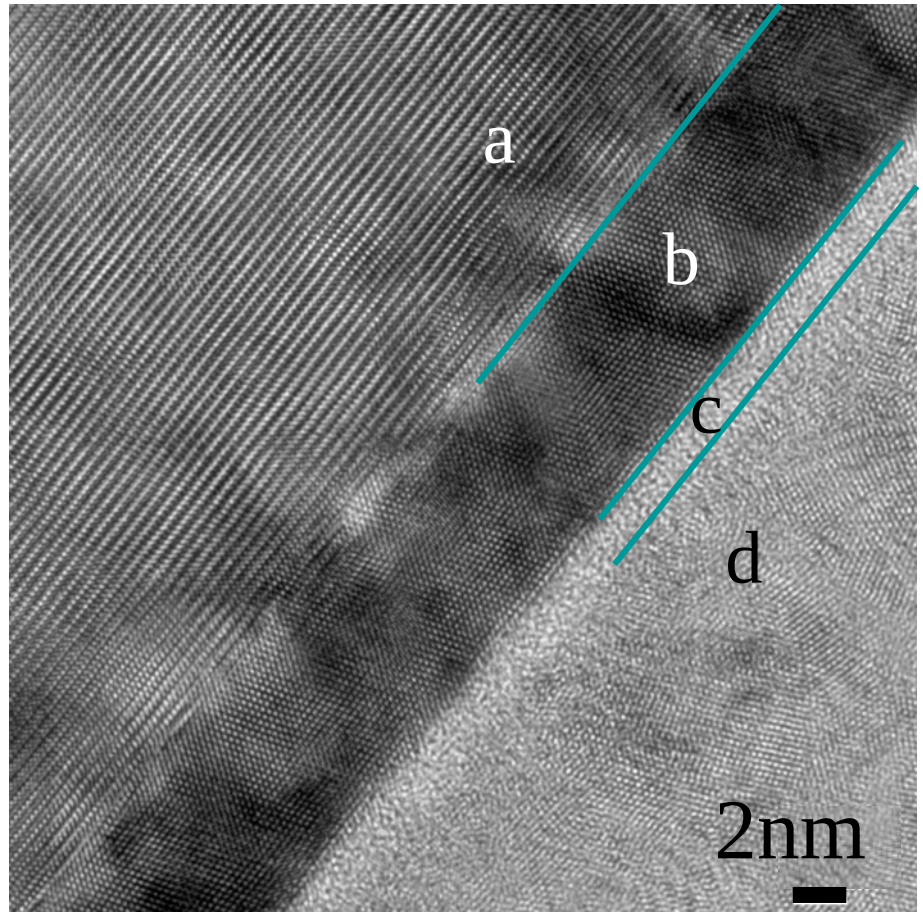

(b)

Fig. 9

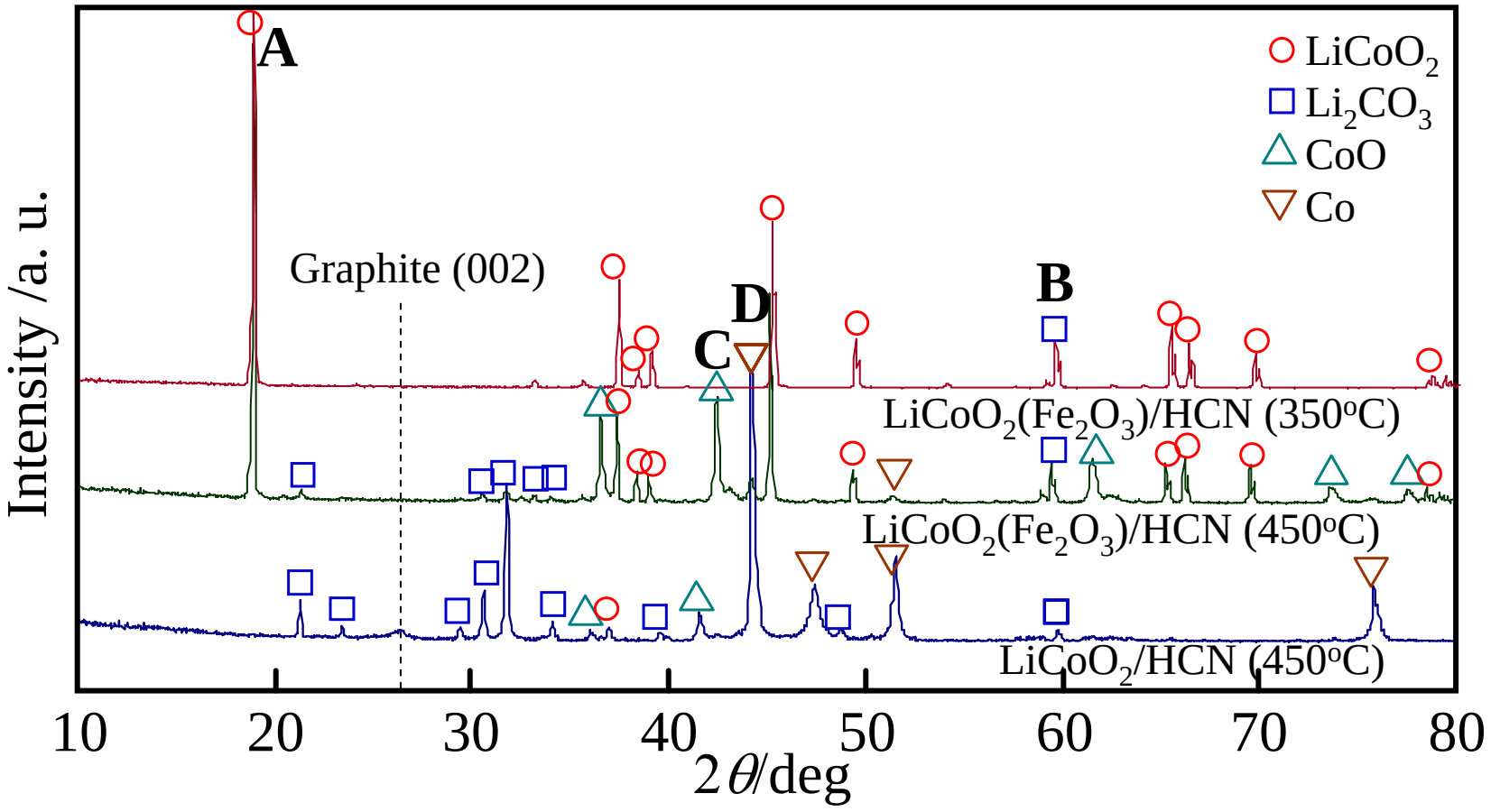
A
B
C
D
Graphite (002)
LiCoO2
Li2CO3
CoO
Co
LiCoO2(Fe2O3)/HCN (350°C)
LiCoO2(Fe2O3)/HCN (450°C)
LiCoO2/HCN (450°C)
Intensity /a. u.
10
20
30
40
50
60
70
80
2θ/deg

Fig. 10

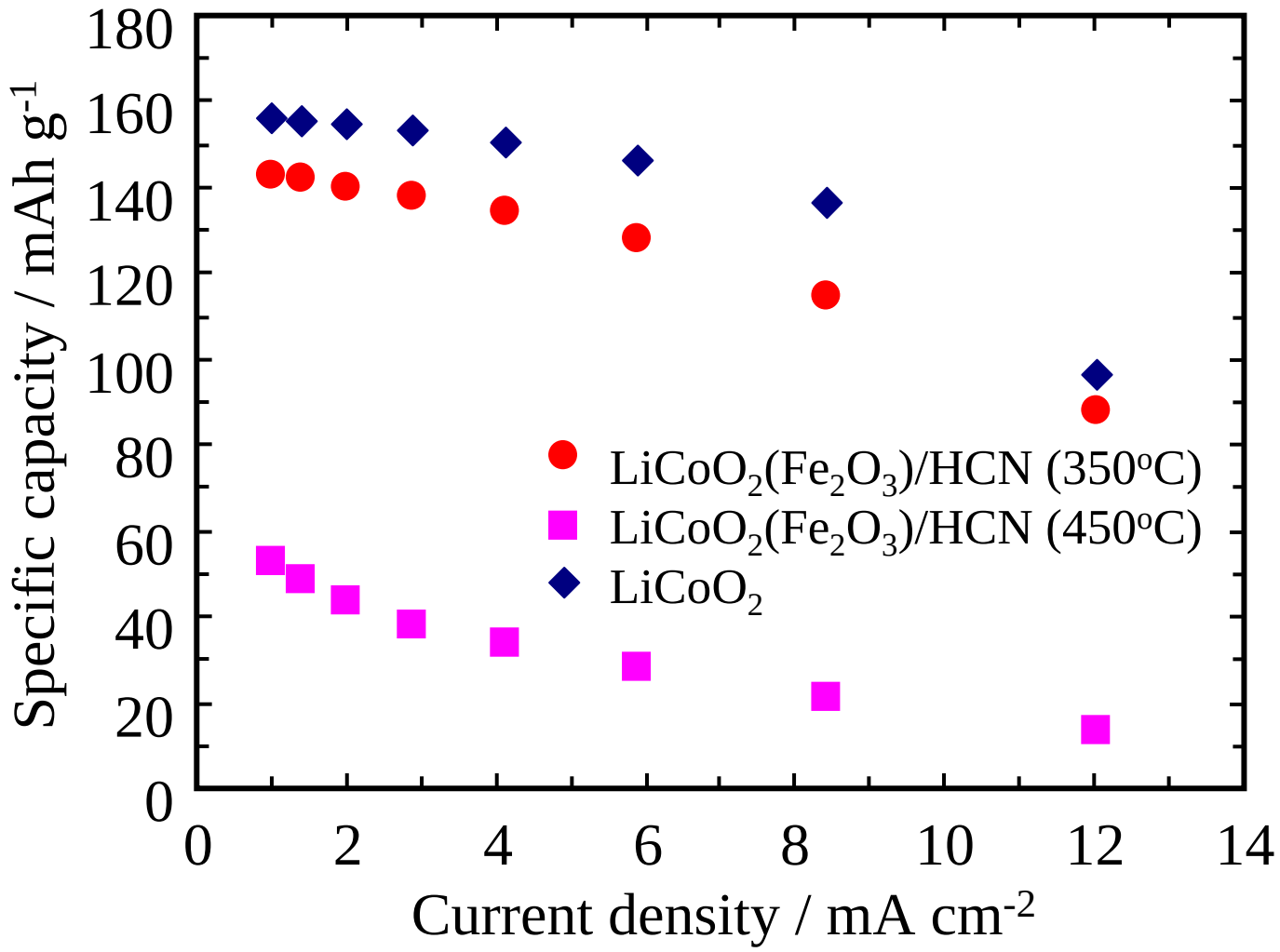
Specific capacity / mAh g-1
180
160
140
120
100
80
60
40
20
0
0
2
4
6
8
10
12
14
Current density / mA cm-2
LiCoO2(Fe2O3)/HCN (350oC)
LiCoO2(Fe2O3)/HCN (450oC)
LiCoO2

Fig. 11

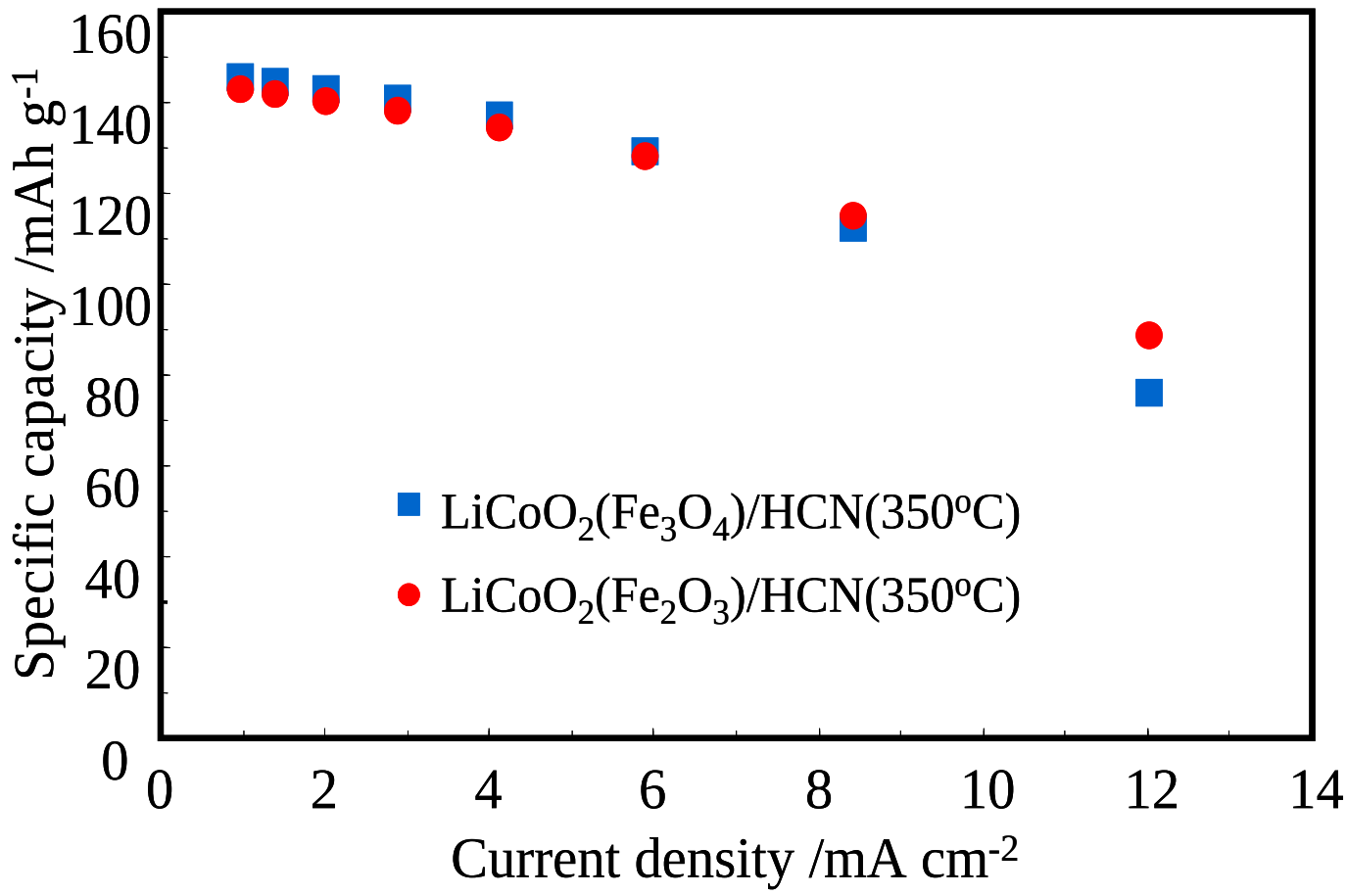
Specific capacity /mAh g-1
160
140
120
100
80
60
40
20
0
0
2
4
6
8
10
12
14
Current density /mA cm-2
LiCoO2(Fe3O4)/HCN(350ºC)
LiCoO2(Fe2O3)/HCN(350ºC)